Chemical Engineering Journal 382 (2020) 122745

Contents lists available at ScienceDirect

Chemical Engineering Journal

journal homepage: www.elsevier.com/locate/cej

Plasma-enabled catalyst-free conversion of ethanol to hydrogen gas and carbon dots near room temperature

Rusen Zhou[a,1], Renwu Zhou[a,c,*,1], Yubin Xian[b,*], Zhi Fang[d], Xinpei Lu[b], Kateryna Bazaka[a,*], Annemie Bogaerts[e], Kostya (Ken) Ostrikov[a]

[a] School of Chemistry, Physics and Mechanical Engineering, Science and Engineering Faculty, Queensland University of Technology, Brisbane, Queensland 4000, Australia
[b] School of Electrical and Electronic Engineering, Huazhong University of Science and Technology, Wuhan 430074, China
[c] School of Chemical and Biomolecular Engineering, The University of Sydney, NSW 2006, Australia
[d] College of Electrical Engineering and Control Science, Nanjing Tech University, Nanjing 210009, China
[e] Research Group PLASMANT, Department of Chemistry, University of Antwerp, Universiteitsplein 1, Wilrijk B-2610, Belgium

HIGHLIGHTS

- New approach for clean hydrogen energy and smart nano-carbons production.
- Effective bioresource conversion using new pulsed plasma modes.
- Catalyst-free, plasma conversion of ethanol at near-room temperature.
- Towards full bioresource utilization: carbon for carbon, hydrogen for hydrogen.

GRAPHICAL ABSTRACT

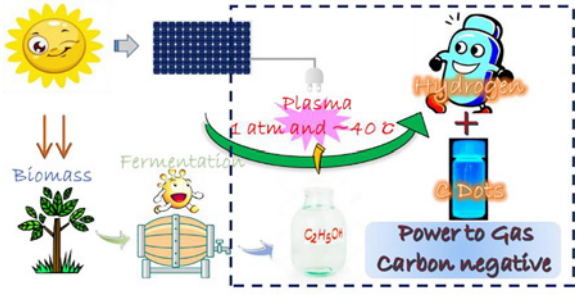

ARTICLE INFO

Keywords:
Non-thermal plasma
Ethanol conversion
Hydrogen
Carbon dots

ABSTRACT

Selective conversion of bio-renewable ethanol under mild conditions especially at room temperature remains a major challenge for sustainable production of hydrogen and valuable carbon-based materials. In this study, adaptive non-thermal plasma is applied to deliver pulsed energy to rapidly and selectively reform ethanol in the absence of a catalyst. Importantly, the carbon atoms in ethanol that would otherwise be released into the environment in the form of CO or CO_2 are effectively captured in the form of carbon dots (CDs). Three modes of non-thermal spark plasma discharges, *i.e.* single spark mode (SSM), multiple spark mode (MSM) and gliding spark mode (GSM), provide additional flexibility in ethanol reforming by controlling the processes of energy transfer and distribution, thereby affecting the flow rate, gas content, and energy consumption in H_2 production. A favourable combination of low temperature (< 40 °C), attractive conversion rate (gas flow rate of ~120 mL/min), high hydrogen yield (H_2 content > 90%), low energy consumption (~0.96 kWh/m^3 H_2) and the effective generation of photoluminescent CDs (which are applicable for bioimaging or biolabelling) in the MSM indicate that the proposed strategy may offer a new carbon-negative avenue for comprehensive utilization of alcohols and mitigating the increasingly severe energy and environmental issues.

* Corresponding authors at: School of Chemistry, Physics and Mechanical Engineering, Science and Engineering Faculty, Queensland University of Technology, Brisbane, Queensland 4000, Australia (R. Zhou and K. Bazaka) and School of Electrical and Electronic Engineering, Huazhong University of Science and Technology, Wuhan 430074, China (Y. Xian).
E-mail addresses: zhourenwu2015@163.com (R. Zhou), yubin.xian@hotmail.com (Y. Xian), kateryna.bazaka@qut.edu.au (K. Bazaka).
[1] These authors contributed equally.

https://doi.org/10.1016/j.cej.2019.122745
Received 26 July 2019; Received in revised form 2 September 2019; Accepted 6 September 2019
Available online 07 September 2019

1. Introduction

Ethanol produced from the conversion of abundant biomass resources such as low-cost non-edible lignocelluloses, is currently contributing for more than 100 billion litres of fuel to the global energy market in an effort to build a more sustainable future [1–3]. Due to its notable advantages including renewability, low toxicity, affordability, ease of storage and high hydrogen content, ethanol has also emerged as a promising feedstock to produce higher-value and cleaner energy carrier, *i.e.* hydrogen (H_2), and is expected to contribute to a more economical and competitive 'hydrogen economy' [4–6].

The most widely studied approaches for converting ethanol into H_2 are steam-based reforming (SR) processes, where vapours of ethanol and water at a specific ratio are introduced into a reactor heated to high temperature (> 700 °C) to enable reactions, such as those in Eqs. (1) and (2), to proceed with or without specially selected or designed catalysts [5,7,8]. As SR of ethanol is a highly endothermic process, large amounts of energy supplied by high temperatures and/or high pressures are needed to drive the reactions. As such, SR processes consume considerable energy and require the use of specific reactors and process control, greatly hindering practical H_2 production [5,9,10]. Although there are other ethanol SR processes achieved via less endothermic reactions (*e.g.* 3–4), with milder reaction conditions, they still have some drawbacks [5,11]. For example, without H_2O or O_2 sustaining the oxidative environment, the formation of coke will negatively affect both the reactors and the catalysts used, while a lower H_2 yield usually has to be a compromise when H_2O or O_2 are used [5,12,13].

$$CH_3CH_2OH + H_2O \rightarrow 2CO + 4H_2 \quad \Delta H_{298\,K} = +256\,kJ/mol \tag{1}$$

$$CH_3CH_2OH + 3H_2O \rightarrow 2CO_2 + 6H_2 \quad \Delta H_{298\,K} = +174\,kJ/mol \tag{2}$$

$$CH_3CH_2OH \rightarrow CO + 3H_2 + C \quad \Delta H_{298\,K} = +71.8\,kJ/mol \tag{3}$$

$$CH_3CH_2OH + 1.8H_2O + 0.6O_2 \rightarrow 4.8H_2 + 2CO_2 \quad \Delta H_{298\,K} = +4.4\,kJ/mol \tag{4}$$

Non-thermal plasma (NTP) is a (partially) ionized gas, usually generated by applying electrical energy to a feeding gas [14–16]. NTP offers a unique physiochemical environment due to the enrichment of the gas with energetic electrons and reactive species, which enables thermodynamically unfavourable reactions to occur under ambient conditions (*e.g.* low temperatures and pressures) [15,17,18]. Importantly, the discharge can be induced and sustained using more and more widely available renewable electricity [19], *e.g.* solar energy, the cost of which is gradually reducing [15,17,19]. As the plasma can be easily switched on/off, it is perfectly suitable for storing fluctuating renewable electricity, providing a solution for the problem of peak shaving and grid stabilization. For these reasons, NTP-based strategies are emerging as an economically-viable family of technologies for various types of material conversion, including ethanol reforming [2,20–22]. Compared to conventional SR, H_2 production from NTP-induced ethanol conversion operates at a significantly lower temperature (< 100 °C) and results in a higher conversion rate (with a H_2 flow rate of several and even more than ten litres per minute) [23,24]. However, the conversion usually has unsatisfactory H_2 selectivity (< 70% v/v) since the reactions initiated by plasma usually lack controllability due to the diversity and high reactivity of plasma-generated species [22–24].

The carbon components in alcohols are ultimately converted to CO_2 in most reported alcohol reforming studies to date [25,26]. Although reforming of ethanol derived from biomass is regarded as a CO_2 neutral process, direct conversion of carbon into high-value carbon materials would make the process greener, more competitive and lower carbon-negative, and as such a more appropriate strategy for mitigating global warming [27]. Recent studies on ethanol being catalytically reformed into H_2 and solid carbon materials (such as nanoporous graphene) offer a novel solution [3,27]. However, temperatures of up to hundreds of degrees (as high as 500 °C) are still required [3]. At the same time, the generation of carbon-based deposits is also fairly common in plasma reforming processes, especially when higher energy is introduced into the system to maintain high conversion rates [2,22,28]. However, the formation of solid-state carbons is usually unwelcome, especially in liquid-phase discharges, because these carbons may lead to not only catalyst deactivation but also to undesirable changes of electrode structures, significantly affecting the performance of the discharges [2,29].

Herein, we describe the development of a high-voltage spark discharge (HVSD) reactor for one-step catalyst-free reforming of bio-renewable ethanol at atmospheric pressure and near room temperature

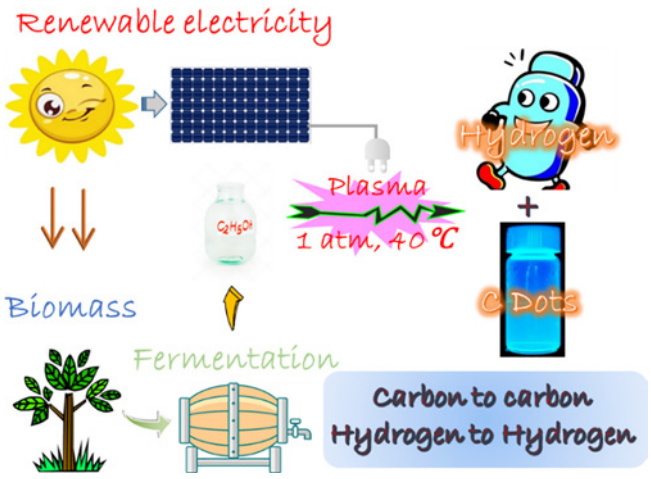

Scheme 1. Illustration of the ethanol reforming process. Ethanol, which can be produced from renewable biomass sources at large scales, represents a promising and environmentally friendly energy carrier. A high-voltage spark discharge (HVSD) reactor is developed for single-step selective catalyst-free conversion of this bio-renewable ethanol at near room temperature into hydrogen and value-added carbon dots (CDs), so as to achieve carbon neutral and comprehensive, potentially 'carbon-to-carbon & hydrogen-to-hydrogen' conversion.

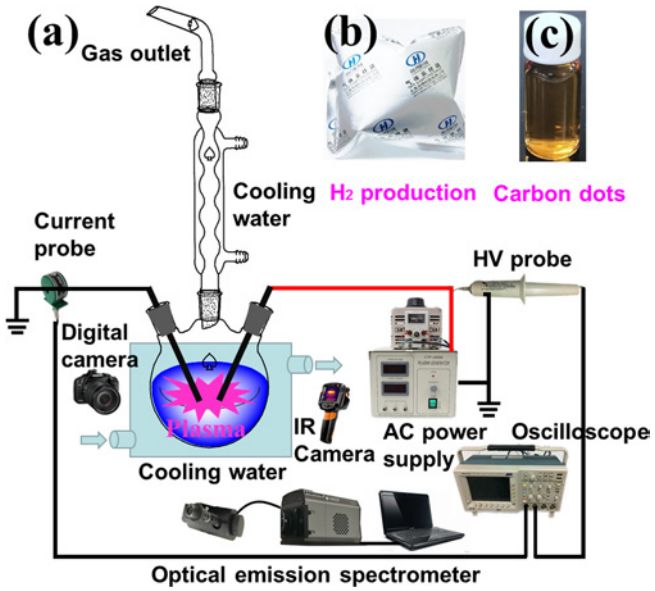

Fig. 1. Plasma reforming system and overview of the process to reform ethanol into hydrogen and carbon dots (CDs). (a) Brief schematic diagram of the plasma reforming setup (the gas collected after passing through an ice-saline water trap and then the total gas flow rate measured by a rotary flowmeter), (b) gas product, and (c) carbon dots in liquid product obtained from 1 h discharge in MSM.

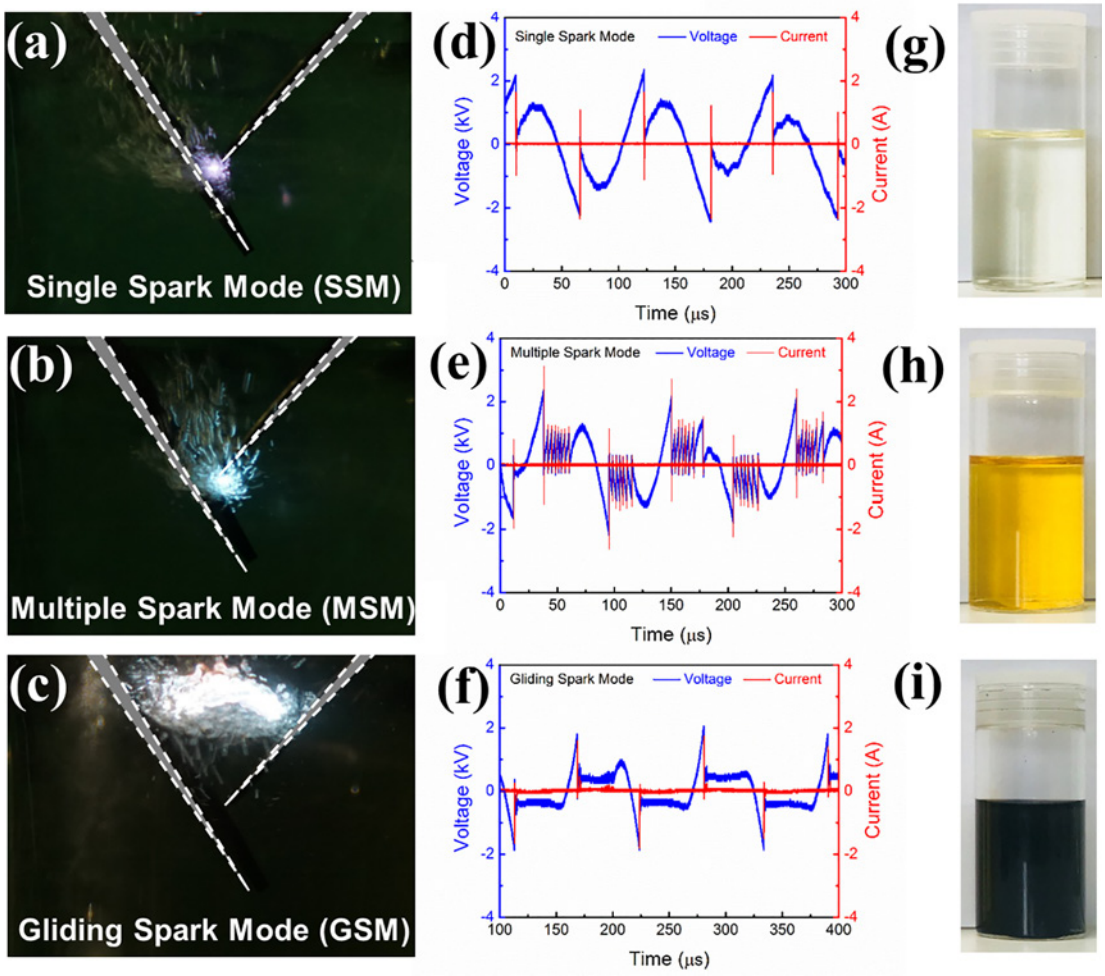

Fig. 2. Photographs of three different plasma discharge modes and their corresponding electrical characteristics (typical applied voltage and current waveforms). (a), (b) and (c) Photograph of single spark mode (SSM), multiple spark mode (MSM) and gliding spark mode (GSM) respectively. Typical applied voltage and current waveforms obtained at a discharge power of 4 (d), 6 (e) and 10 W (f). Photograph of ethanol after 1 h reforming using SSM (g), MSM (h) and GSM (i).

(Scheme 1). Three modes of plasma discharges can be obtained by just varying the amount of energy put into the system and the main features of these discharges are concluded and compared in ethanol conversion, which achieves higher yeild and selectivity of hydrogen. The radicals generated from HVSD in ethanol solution are studied, and the processes of hydrogen and carbon dots (CDs) production are also speculated. Moreover, the obtained CDs are characterised and successfully applied in the biological applications as a agent for cell imaging.

2. Materials and methods

2.1. Non-thermal plasma reforming reactor

A 250 mL, three-necked, double-walled, round-bottomed flask is adopted as the plasma reforming reactor for the conversion (Fig. 1). 150 mL ethanol is contained in it. A spherical condenser supplied with cooling water is connected to the flask to preliminarily condense unreacted ethanol vapor. Two tungsten needles (diameter 2 mm) are put into the flask through the two side-necks to work as electrodes with one connected to AC high voltage and one grounded. The angle between the needles is around 60°. The gap between the tips of the needles is about 1 mm. An AC power supply (TCP-2000K, Najing Suman Electronic, China) capable of supplying bipolar AC output with the peak-peak voltage ($V_{p\text{-}p}$) of 0–30 kV at an AC frequency of 9.0 kHz is used to drive the discharge. When high voltage is applied on the HV electrode, spark discharge is directly ignited between the tips of the two electrodes in ethanol solution and the corresponding discharge power is calculated to be 4, 6 and 10 W. The real-time temperature of the solution is measured by an infrared thermometer.

2.2. Electrical and optical measurements

Analysis of spark discharge mainly consists of U-I characteristics, spectral characteristics and discharge images. To measure the discharge current and the applied voltage, a current probe (Pearson 4100) and a high voltage probe (Pintech P6039A) are used. Based on the U-I characteristics, energy of spark discharge and energy consumption can be calculated. Optical emission diagnostic (OES) is carried out to understand the formation of chemical species in on-board hydrogen production system at first instance of plasma being discharged. OES from the discharge region were obtained using a spectrograph (ANDOR SR-500i-A-R spectrometer) with a resolution of 0.5 nm in the wavelength range of 200 to 1000 nm.

2.3. Analysis of gaseous and liquid products

The gaseous products are gathered after passing through an ice-saline water (30% NaCl) trap to further condense ethanol and water vapor. Flow rate of total gas is measured by a rotary flowmeter and the components of thus-obtained gas are analysed using a gas chromatograph (GC) (GC-2014, Shimadzu) equipped with a thermal conductivity detector (TCD) and a flame ionized detector (FID), calibrated for a

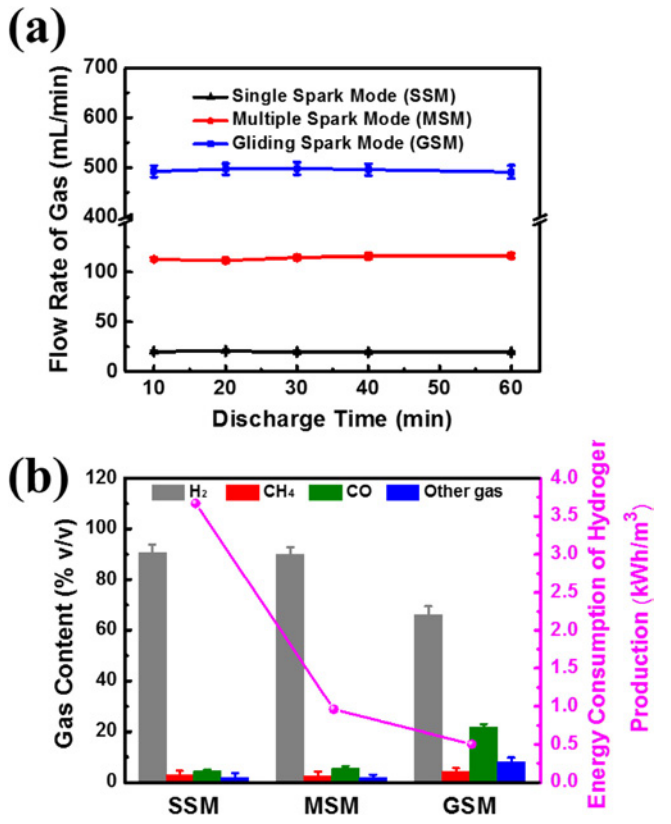

Fig. 3. (a) The change of flow rate of total gas over time (first hour) in SSM, MSM, and GSM, (b) gas content and energy consumption in H_2 production in SSM, MSM, and GSM.

serial concentraions of each gaseous products using standard gas mixtures and other calibrated gas mixtures [4]. The content of each specific gaseous component is defined as volume percentage to the total gas flow.

Liquid products are analyzed by GC–MS using an Agilent 6890 Series Gas Chromatograph with an Aglient HP-5 column, and a HP 5975 mass spectrometer detector with helium as a carrier gas. A splitless injection of 1 μL is delivered to the injection port set at 250 °C. The initial temperature is set at 90 °C, with a heating rate of 5 °C/min to a temperature at 250 °C. The samples are heated at 250 °C for 3 min. Compounds are identified by means of the Wiley library-HP G1035A and NIST library of mass spectra and subsets-HP G1033A.

2.4. Characterization of thus obtained carbon dots

After discharge, the liquid is purified using a dialysis tube and then oven-dried overnight to get carbon dots (CDs) [30]. The CDs are characterized using transmission electron microscope (TEM, JEOL 2100, Japan), Raman spectroscopy (Jobin Yvon Lab RAM HR 800 UV micro-Raman spectrometer, France), X-ray photoelectron spectroscopy (XPS, AXIS SUPPA (KRATOS)) equipped with an Al (K_α = 1486.6 eV) X-ray as excitation source, and Fourier transform infrared (FTIR)

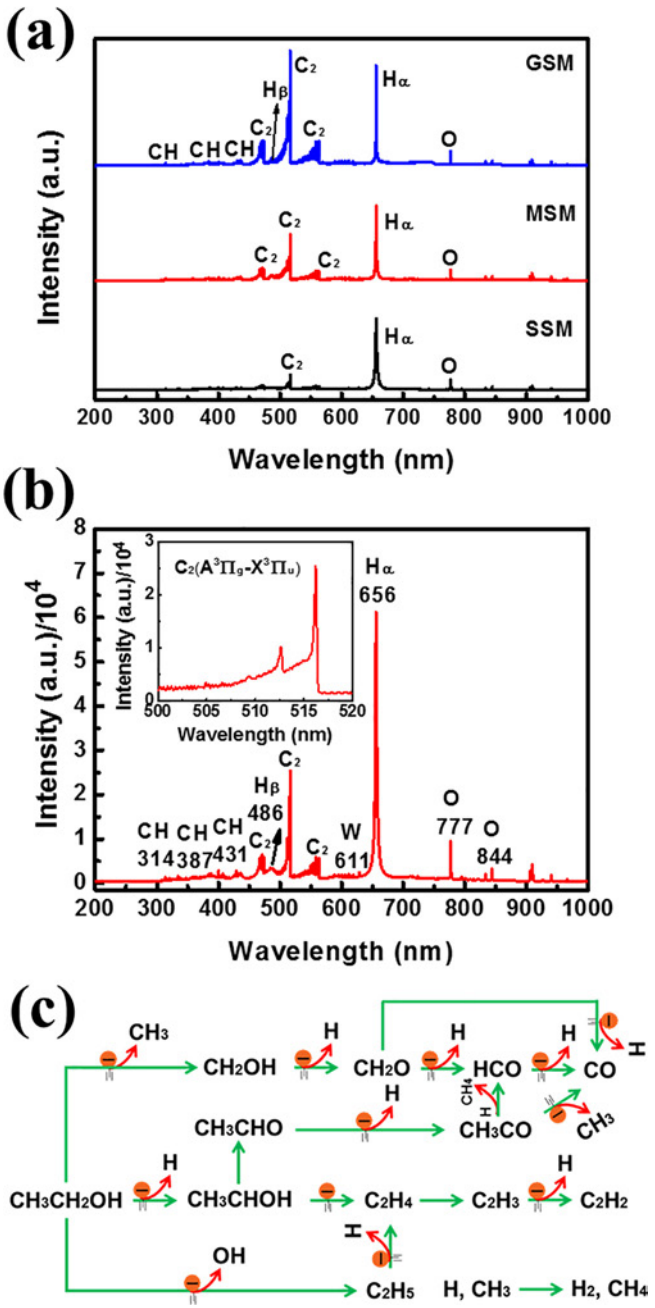

Fig. 4. (a) Measurement of optical emission spectrum (OES) characteristics in SSM, MSM and GSM, and (b) enlarged figure of OES from MSM, inserted with the enlarged region of 500–520 nm. (c) Possible mechanisms of dissociative pathways of ethanol conversion.

spectrum (Nicolet iS10, Thermo Scientific, USA) using an attenuated total reflection (ATR) diamond probe as IRE. Optical vibration spectra are obtained from ultraviolet–visible (UV–vis) adsorption spectroscopy (Cary 60, Agilent, USA) and fluorescence spectroscopy (Cary Eclipse-

Table 1
Specific features of the three plasma discharge modes, including the generated products, way of energy transfer and summary of achievements.

Mode	Gas products (vol%)					Carbon products	Energy transfer	Achievements
	H_2	CH_4	CO	CO_2	Other gas			
SSM	90.8	2.8	4.5	–	1.9	–	Singe self-pulsed discharge	(Slow) H_2 (> 90% of purity) production
MSM	90.1	2.6	5.5	–	1.8	CDs	6 self-pulsed discharges	Selective and rapid generation of H_2 (> 90% of purity) and CDs.
GSM	66.0	4.2	21.7	1.3	6.8	Solid Carbon	30 μs continous discharges	Fast syngas (H_2 + CO) production

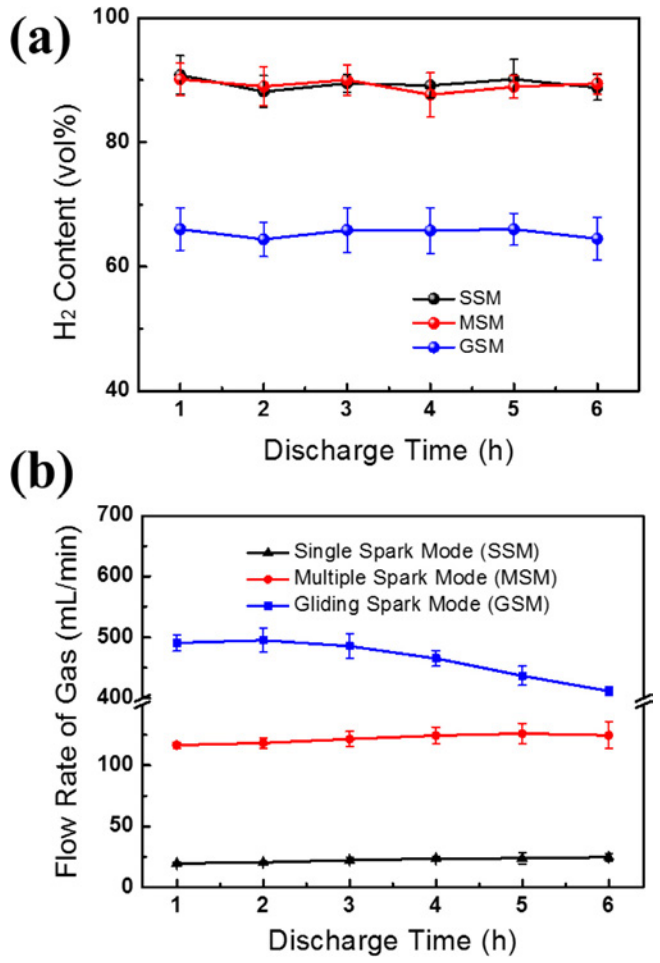

Fig. 5. The content of hydrogen gas (a) and the total flow rate of gas (b) generated in SSM, MSM and GSM over a discharge time of up to 6 h.

2006, Varian, Australia).

2.5. Procedure for cell viability and cell imaging

MDA-MB-468 cells are seeded at a density of 1.0×10^5 cells in a 96-well plate and cultured for 24 h at 37 °C with 5% CO_2 in DMEM with 10% FCS. Then, CDs are introduced into the wells in the concentrations of 0, 100, 200, 400 and 800 μg mL^{-1} and incubated for 4 h at 37 °C. Following incubation of cells with the indicated treatments, Hoechst (1 μg mL^{-1}) is added 30 min before imaging. Cells are imaged on an IN Cell Analyzer 2200 (GE Healthcare; 40 × objective). Live/dead cell analysis is performed using IN Cell analysis software.

3. Results and discussion

3.1. Electrical characteristics of the plasma reforming system

Fig. 2 shows the three different plasma discharge modes, termed single spark mode (SSM), multiple spark mode (MSM) and gliding spark mode (GSM), respectively, achieved in liquid ethanol with corresponding discharge power of 4, 6 and 10 W (with enlarged U-I waveforms detailed in Fig. S1). It is well known that compared to the corona discharge, spark discharges in liquid have longer discharge channels and higher partial discharge intensity; while compared with reactive arc discharge, they usually require lower energy input, making themselves more suitable for inducing reactions in liquids [22,23]. Clearly, in the initial discharge state at a lower discharge power of 4 W, a purple-coloured plasma (Fig. 2a) is generated. The voltage and current shown in Fig. 2d indicate that a single pulsed microdischarge occurs in a half cycle, and the discharge duration in most cases is tens of nanoseconds (Fig. S1a), a phenomenon that is referred to as a single spark mode (SSM) discharge. When the discharge power is increased from 4 W to 6 W, the colour of plasma changes to azure (Fig. 2b). Voltage and current shown in Fig. 2e confirm that an initial pulse discharge is followed by ~6 self-pulsing discharges in every half cycle, with the process referred to as a multiple spark mode (MSM) discharge. When the discharge power is further increased to 10 W, the discharge mode changes to a gliding spark mode (GSM) discharge (Fig. 2c), with brighter light emission and larger spatial distribution of the plasma. The discharge ignites at the tip of the electrode, then rises along the area between the electrodes. Fig. 2f and the enlarged section of voltage and current waveforms shown in Fig. S1c reveal that the discharge in GSM lasts for more than 30 μs in every half cycle.

3.2. Effects of discharge modes on ethanol reforming

When plasma is introduced into the system, reactions related to ethanol conversion can take place at room temperature, resulting in the production of gas-phase chemicals, including H_2, CO, CH_4 and other gases like CO_2, C_2H_4 and C_2H_2, with hydrogen being the major product [2,22–24]. The total gas flow rate as a function of discharge time (the first 60 min) in these three kinds of discharge modes is presented in Fig. 3a. It is observed that discharge time has little impact on the total gas flow rate in the each discharge mode, but the types of discharge modes have a significant effect on the gas flow rate. Compared with the total gas flow rate in SSM (~20 mL/min), the value increased significantly for the other modes, specifically more than 5 times (~116 mL/min) in MSM and around 24 times in GSM (~500 mL/min). This result indicates an improvement in the density of this well-controlled plasma when discharge power increases from 4 W to 10 W, which is consistent with the results obtained from the applied voltage and current waveforms. The gas content (average values of gas samples collected at 30 and 60 min discharge) as a function of the input power is presented in Fig. 3b. On the contrary, both gas flow rate and content depend on the spark discharge mode (Table 1). In SSM, the content of H_2, CH_4 and CO in gas phase is 90.8%, 2.8%, and 4.5%, respectively, and their corresponding content in MSM is 90.1%, 2.6% and 5.5%. In GSM, the H_2 content decreases to 66.0%, and that of CH_4 and CO is 4.2% and 21.7%, respectively. The content of other gases in GSM is ~8.1%; to be specific, the gas mainly consists of CO_2 (1.3%), which is almost undetectable in both SSM and MSM, and hydrocarbons with low molecular weight like C_2H_6, C_2H_4 and C_2H_2, the generation of which usually leads to the formation of carbon deposits in non-thermal plasma (NTP)-associated conversions, with possible reactions listed in Table S1.

The variation of solution temperature with processing time is presented in Fig. S2. The results reveal that the thermal effect during the ethanol conversion in all three modes is insignificant, resulting in only a slight increase in the liquid temperature with discharge time greater than 15 min to 37, 38 and 40 °C in the case of SSM, MSM and GSM, respectively. In other thermal-based conversions, all molecules usually need to be heated to a high temperature, although in many cases the ones involved in the chemical bond cleavage or other reactions are very limited. However, the energy from non-thermal plasma (NTP) is generally limited in a specific region, mainly for heating and accelerating the free electrons, boosting the materials inside to be converted while mitigating the increase of the temperature in the whole system especially in liquid-phase conversions [2]. Without strong signs of temperature increase being witnessed even with extended time of operation here proves that most of the pulse energy is selectively delivered to reform ethanol and thus indicates the requirements for temperature and heat-transfer control can be significantly simplified in practical applications, *e.g.* on-board H_2 generation for fuel cells in new energy vehicles.

The energy consumption of hydrogen production is defined as the

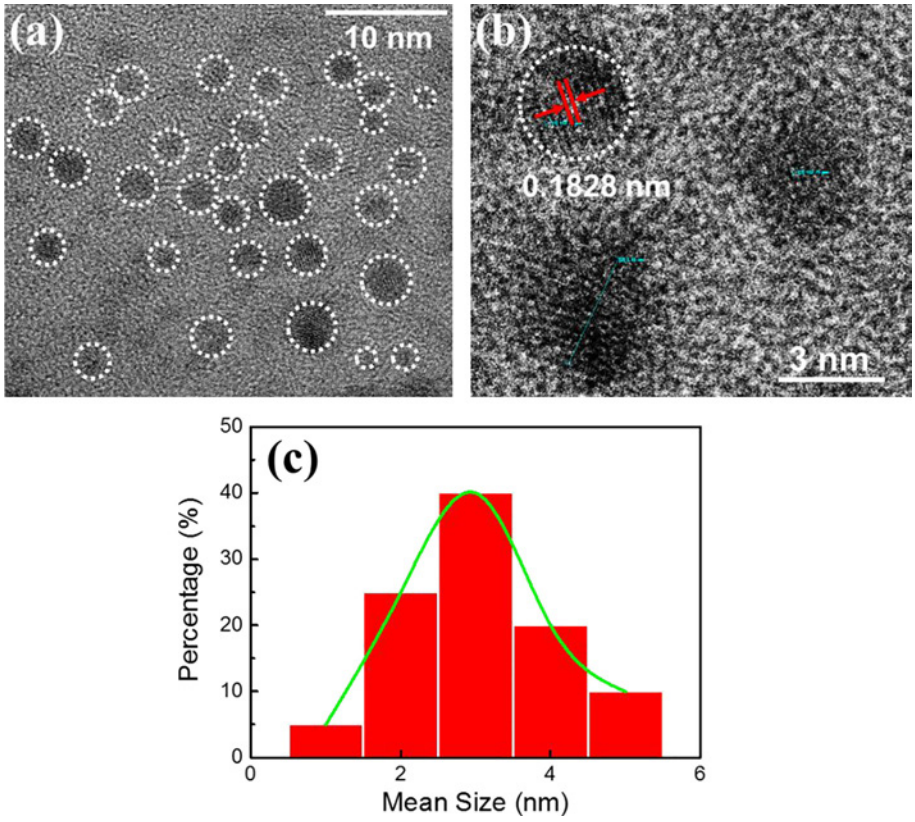

Fig. 6. Structural and optical characterization of CDs. TEM image (a), high-resolution TEM image (b) and size distribution of CDs from TEM image (c). CDs were obtained from 1 h discharge in MSM.

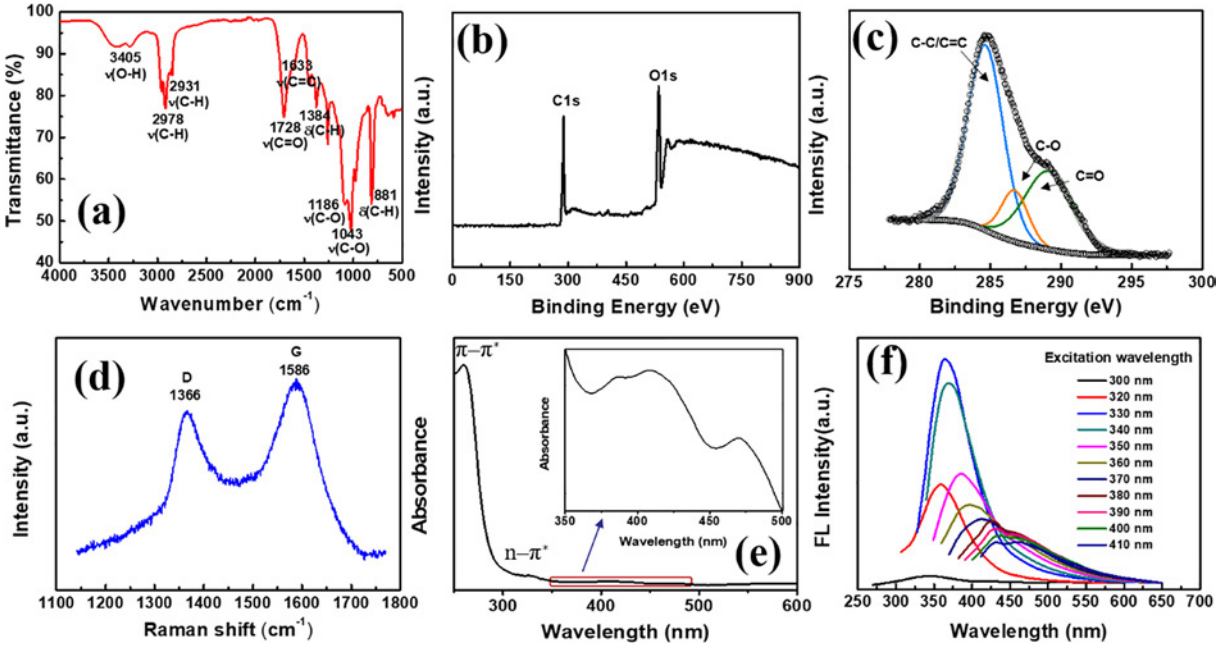

Fig. 7. FT-IR spectrum (a), XPS survey spectrum (b), high-resolution C1s XPS spectrum (c), Raman spectrum (d), UV–vis spectrum with enlarged spectrum in the region of 350–500 nm inserted (e) and FL spectra (f) of the CDs obtained from 1 h discharge in MSM.

value of the energy consumed to produce 1 m^3 of H_2. In this investigation, the energy consumption of hydrogen production reaches 3.67 and 0.96 kWh/m^3 in SSM and MSM, and displays the lowest value in the case of GSM (0.50 kWh/m^3) (Fig. 3b). By comparison with other methods of hydrogen production from ethanol or ethanol solution by using different forms of discharge such as the efficient microwave plasma [31] (Table S2), GSM stands out as a good candidate for both cost- and time-effective production of H_2 and more precise syngas (H_2 and CO), while MSM shows excellent performances in enhancing the H_2 content with still good conversion rate and energy consumption. Moreover, although the H_2 content in all of the three modes shows little variation as a function of discharge time prolonged to 6 h, the gas flow

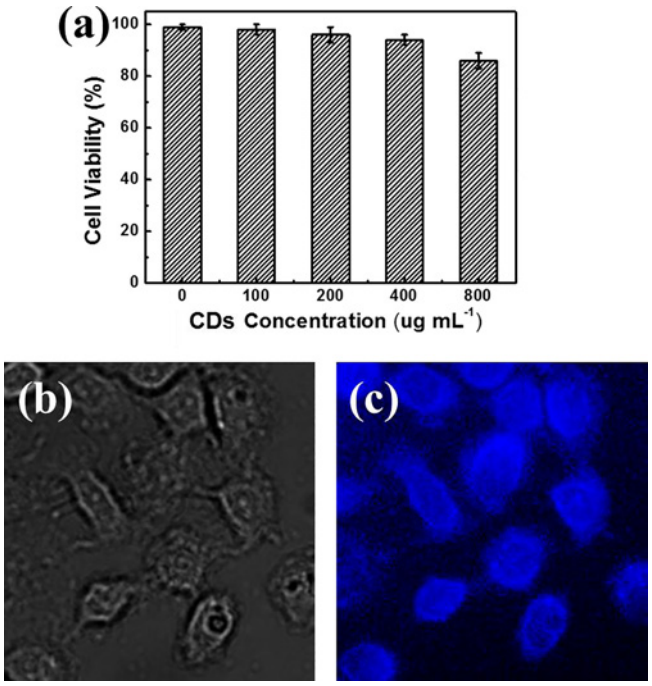

Fig. 8. (a) Cell viability values (%) estimated by live-dead assay in MDA-MB-468 breast cancer cells, which are incubated with serial concentrations of the CDs for 48 h at 37 °C. Images of a bright-field (a) and confocal fluorescence of MDA-MB-468 cells incubated with CDs at the concentration of 400 μg/mL (excited by 330 nm).

rate of gas changes (Fig. 5). To be specific, the conversion rate in the GSM decreases especially after discharging for 3 h and onwards (and the discharge becomes more difficult to achieve), with a total gas flow rate of ~412 mL/min at 6 h, while a slight increase (by ~5 mL/min) in the rate is witnessed both in the case of MSM and SSM (no solid-state products observed in the whole process). This suggests that the deposited carbon in GSM may induce undesirable effects into the conversion process, with the effects accumulating along with the processing time. From the viewpoint of practical applications, MSM is highly promising for hydrogen production in liquid for long-time operation.

3.3. Possible dissociative pathways of plasma-enabled ethanol conversion

Many radicals can be formed in the process of spark discharge and these active species may play an important role in hydrogen production. Optical emission spectroscopy (OES) is a non-interfering and direct approach to understand the generation of intermediates during the gas discharge (Fig. 4a and b). Similar gas emission spectra for the discharge from SSM, MSM and GSM indicate the generation of similar free radicals, while the intensity of almost all bands decreases in the sequence of GSM, MSM and SSM, with the decrease being directly associated with the amount of energy put into the system and conversion reactivity [22,23,32]. For example, the higher intensity of the atomic hydrogen line (H_β at 486 nm and H_α at 656 nm) is usually associated with the faster formation of H_2 [23]. The Swan bands at 436–438, 512–516, and 547–563 nm, *i.e.* a characteristic band of C_2 associated with the recombination of carbon atoms, is closely linked to the production of hydrocarbon compounds, carbon deposition and carbogenic nuclei, which may favour the formation of carbon dots in the solution [28,33]. This hypothesis is also confirmed by the physical state changes of the solution after reforming shown in Fig. 2g–i. After 60 min discharge, the color of ethanol in SSM slightly turns into pale thin yellow, and brown yellow in GSM, while the colour in the GSM is brownish black with visible solid-state carbon inside.

The reforming of alcohols using NTP-enabled techniques is generally accomplished in two stages: electron bombardment and free radical induced reactions (summarized in Table S1, with general possible conversion pathways shown in Fig. 4c) [2,4,32]. Once high voltage is applied, a large number of electrons are generated, which are then accelerated in the strong electric field (~3 to 20 eV in discharge channels) [2]. The energetic electrons then bombard the nearby substances (in this case, ethanol molecules), with the interaction leading to excitation of these molecules and/or their fragmentation due to scission of covalent bondings, and to the formation of free radicals (*e.g.* ·H, CH_3CH_2O·, CH_3CH_2·, ·CH_2OH, ·CH_3, ·OH, etc.) [24,32]. These radicals, together with various excited species, will further induce a series of radical collisions at high rates to obtain the targeted products as well as to boost electron generation needed to sustain the whole process [4,23,32]. As discharge power increases (in the case of GSM), the electric field strength between the electrode tips increases, which leads to the generation of more energetic electrons and also enables high-energy electrons to obtain greater energy to collide with ethanol molecules and produce more oxidative species (O and OH) to participate in the reactions of H_2 production, resulting in increased CO production [22,24,33,34]. Moreover, the plasma density is also significantly increased due to the enhanced input energy in GSM, where the electron temperature and density and the free radical density are expected to be much higher than in SSM and MSM, contributing to a significantly faster conversion and formation of other C-containing gases [32,35].

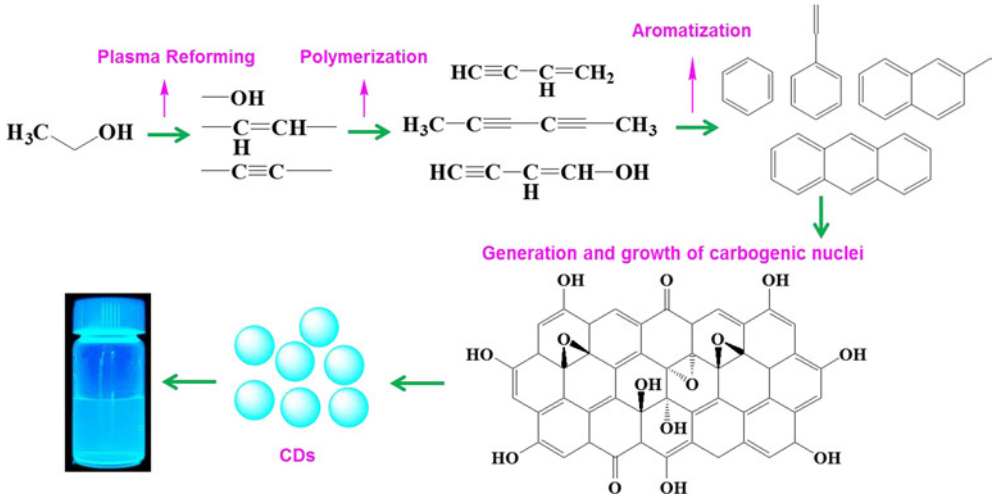

Fig. 9. A proposed formation mechanism of graphene quantum dots (CDs) from ethanol solution in plasma reforming system.

3.4. Characteristics of carbon dots produced from MSM

Obviously different from the case of GSM, where most of the carbon atoms in ethanol are converted to gaseous CO and solid deposited carbon, carbon is retained in the liquid in the form of photoluminescent carbon dots (CDs) in MSM (summarized in Table 1). After 1 h reforming in MSM, the residual liquid product is purified using a dialysis tube before the remaining ethanol is evaporated to obtain the targeted CDs for further characterization. Transmission electron microscopy (TEM) image and high-resolution TEM images and the corresponding particle size distribution (PSD) of the produced CDs are shown in Fig. 6. It can be seen that the CDs have a circular or oval morphology with a uniform particle size of less than 5 nm (with PSD peak around 3 nm) and the lattice distance in the CDs is 0.18 nm, which belongs to the (1,0,2) plane of graphite [30,36–38]. Fourier transform infrared (FT-IR) analysis is used to investigate the surface functional groups of the CDs. The FTIR spectra in Fig. 7a indicate the presence of −OH functional groups, C═C bonds, C−H and C−O stretching, C−C vibration, as well as a peak at 1384 cm^{-1} which could be indicative of a C−O−C asymmetric stretch or C−H bending arising from a methyl functional group [39,40]. The chemical composition of the CDs is identified by X-ray photoelectron spectroscopy (XPS) spectra. The full-scale spectrum in Fig. 7b confirms the existence of carbon (62.6%), and oxygen (37.4%). The high-resolution spectrum of C1 s in Fig. 7c reveals the presence of C−C/C═C (284.5 eV), C-O (286.3 eV), and C═O (288.5 eV). The Raman spectrum shown in Fig. 7d features two peaks at 1366 and 1586 cm^{-1}, corresponding to the disordered sp^3 carbon (D-band) and well-ordered graphite sp^2 carbon (G-band)-hybridization structure of the CDs, respectively [30,36,37]. It can be concluded that the obtained CDs possess a reasonably low number of lattice defects according to the higher strength of the G peak compared to the D peak. The UV–vis adsorption spectrum of the CDs in Fig. 7e suggests that the CDs feature three main adsorption bands. The intensive one sits at ~260 nm attributed to π–π^* transition; the small shoulder at ~320 nm is usually assigned to n–π^* transition, while a weak band at 400–420 nm results from the functionalized surface states of the obtained CDs [30,36–39]. Fluorescence (FL) spectra of the CDs are depicted in Fig. 7f, illustrating the FL property dependent on the excitation wavelength. The strongest peak centred at 365 nm is achieved with 330 nm excited, and gradual red-shifts (365 to 465) of the peak are witnessed with the excitation wavelength tuned from 330 to 410 nm.

3.5. Biomedical applications of thus-obtained carbon dots

Additionally, experiments are further conducted to demonstrate the potential of using thus-obtained CDs for biological applications. The applicability of the CDs for bioimaging or biolabelling in cancer cells, and the cytotoxicity, a key factor considered for materials used for biomedical applications, are measured by using breast cancer cells (MDA-MB-468). As shown in Fig. 8a, the cell viability stands over 95% when the concentration of CDs varies from 100 to 400 μg/mL, and the value is still as high as 86% even when the CD concentration is increased up to 800 μg/mL, indicating low cytotoxicity and outstanding biocompatibility of the CDs generated by MSM plasma conversion of ethanol. Thus-generated CDs can also be used for cell bioimaging, as demonstrated by confocal visualisation of the MDA-MB-468 cells treated with CDs, with the results shown also in Fig. 8b and c. The cells can be uniformly stained by the CDs and exhibit a clearer morphology (excited by 330 nm) compared to that in the bright field, suggesting the applicability of the CDs for bioimaging or biolabelling [36–38].

Finally, to investigate the formation process of CDs in ethanol during plasma reforming using MSM, GC–MS is applied to identify the intermediates in the liquid after CDs removal. Clearly, compounds (with carbon number > 3) turn up (shown in Fig. S3), indicating that not only decomposition reactions, but also polymerizations occur in this system with various aromatic hydrocarbons generated. Based on the above observations and previous studies of formation of carbogenic materials from small molecules, a plausible reaction mechanism of CDs formation is proposed, as shown in Fig. 9 [37–41]. In the first stage, dehydrogenation (oxidation) of ethanol takes place in the presence of plasma-induced highly energetic electrons, yielding diverse radicals such as unsaturated alkenes (−CH═CH−), and alkynes (−C≡C−). Subsequently, the labile unsaturated hydrocarbons acting as new carbon sources covalently interact with each other and form aromatic rings, the elementary unit of the graphene structure. Finally the carbogenic nuclei increase in size and ultimately form CDs.

4. Conclusion

In summary, the concept of integrated reforming of ethanol into value-added products near room temperature by means of non-thermal plasma is highly promising. This study reveals that by simply controlling the input energy, non-thermal spark discharge can be used as an effective method for the simultaneous reforming of ethanol into H_2 and high-value carbon dots at low temperature (< 40 °C) with an attractive conversion rate and in the absence of any catalyst. Moreover, the as-synthesized CDs with low cytotoxicity have been successfully applied in biological applications, *e.g.*, as a agent for cell imaging. Furthermore, with bio-ethanol becoming more widely available from biomass conversion, and at the same time renewable electricity (from *e.g.* solar) used to drive the non-thermal plasma discharge becoming more cost-competitive, this study provides a step towards the development of carbon-negative and cost-effective strategies for both green energy generation and comprehensive utilization of bio-resources.

Appendix A. Supplementary data

Supplementary data to this article can be found online at https://doi.org/10.1016/j.cej.2019.122745.

References

[1] M.S. Pino, R.M. Rodríguez-Jasso, M. Michelin, A.C. Flores-Gallegos, R. Morales-Rodriguez, J.A. Teixeira, H.A. Ruiz, Bioreactor design for enzymatic hydrolysis of biomass under the biorefinery concept, Chem. Eng. J. 347 (2018) 119–136.
[2] C. Du, J. Mo, H. Li, Renewable hydrogen production by alcohols reforming using plasma and plasma-catalytic technologies: challenges and opportunities, Chem. Rev. 115 (2014) 1503–1542.
[3] G.F. Han, Z.W. Chen, J.P. Jeon, S.J. Kim, H.J. Noh, X.M. Shi, F. Li, Q. Jiang, J.B. Baek, Low-temperature conversion of alcohols into bulky nanoporous graphene and pure hydrogen with robust selectivity on CaO, Adv. Mater. 31 (2019) 1807267.
[4] L. Wang, S. Liu, C. Xu, X. Tu, Direct conversion of methanol to nC_4H_{10} and H_2 in a dielectric barrier discharge reactor, Green Chem. 18 (2016) 5658–5666.
[5] T. Hou, S. Zhang, Y. Chen, D. Wang, W. Cai, Hydrogen production from ethanol reforming: catalysts and reaction mechanism, Renew. Sustain. Energy Rev. 44 (2015) 132–148.
[6] H.Y. Lian, J.L. Liu, X.S. Li, X.B. Zhu, A.Z. Weber, A.M. Zhu, Plasma chain catalytic reforming of methanol for on-board hydrogen production, Chem. Eng. J. 369 (2019) 245–252.
[7] W. Mulewa, M. Tahir, N.A.S. Amin, MMT-supported Ni/TiO2 nanocomposite for low temperature ethanol steam reforming toward hydrogen production, Chem. Eng. J. 326 (2017) 956–969.
[8] G. Deluga, J. Salge, L. Schmidt, X. Verykios, Renewable hydrogen from ethanol by autothermal reforming, Science 303 (2004) 993–997.
[9] Y.C. Sharma, A. Kumar, R. Prasad, S.N. Upadhyay, Ethanol steam reforming for hydrogen production: latest and effective catalyst modification strategies to minimize carbonaceous deactivation, Renew. Sustain. Energy Rev. 74 (2017) 89–103.
[10] M. Nielsen, E. Alberico, W. Baumann, H.-J. Drexler, H. Junge, S. Gladial, M. Beller, Low-temperature aqueous-phase methanol dehydrogenation to hydrogen and carbon dioxide, Nature 495 (2013) 85–89.
[11] H. Zabed, J. Sahu, A. Boyce, G. Faruq, Fuel ethanol production from lignocellulosic biomass: an overview on feedstocks and technological approaches, Renew. Sustain. Energy Rev. 66 (2016) 751–774.
[12] E.B. Pereira, P.R. de la Piscina, S. Martí, N. Homs, H_2 production by oxidative steam reforming of ethanol over K promoted Co-Rh/CeO_2-ZrO_2 catalysts, Energy Environ. Sci. 3 (2010) 486–492.
[13] R. Guil-López, R. Navarro, M. Peña, J. Fierro, Hydrogen production by oxidative ethanol reforming on Co, Ni and Cu ex-hydrotalcite catalysts, Int. J. Hydrogen Energy 36 (2011) 1512–1523.
[14] L. Wang, Y. Yi, C. Wu, H. Guo, X. Tu, One-step reforming of CO_2 and CH_4 into high-value liquid chemicals and fuels at room temperature by plasma-driven catalysis,

Angew. Chem. Int. Ed. 56 (2017) 13679–13683.
[15] R. Zhou, R. Zhou, K. Prasad, Z. Fang, R. Speight, K. Bazaka, K.K. Ostrikov, Cold atmospheric plasma activated water as a prospective disinfectant: the crucial role of peroxynitrite, Green Chem. 20 (2018) 5276–5284.
[16] I. Levchenko, K. Bazaka, O. Baranov, R.M. Sankaran, A. Nomine, T. Belmonte, S. Xu, Lightning under water: diverse reactive environments and evidence of synergistic effects for material treatment and activation, Appl. Phys. Rev. 5 (2018) 021103.
[17] X. Pei, D. Gidon, Y.J. Yang, Z. Xiong, D.B. Graves, Reducing energy cost of NO_x production in air plasmas, Chem. Eng. J. 362 (2019) 217–228.
[18] A. Bogaerts, E.C. Neyts, Plasma technology: an emerging technology for energy storage, ACS Energy Lett. 3 (2018) 1013–1027.
[19] K. Li, J.L. Liu, X.S. Li, H.Y. Lian, X. Zhu, A. Bogaerts, A.M. Zhu, Novel power-to-syngas concept for plasma catalytic reforming coupled with water electrolysis, Chem. Eng. J. 353 (2018) 297–304.
[20] S. Liu, D. Mei, L. Wang, X. Tu, Steam reforming of toluene as biomass tar model compound in a gliding arc discharge reactor, Chem. Eng. J. 307 (2017) 793–802.
[21] R. Zhou, R. Zhou, X. Zhang, Z. Fang, X. Wang, R. Speight, H. Wang, W. Doherty, P. Cullen, K. Ostrikov, K. Bazaka, High-performance plasma-enabled biorefinery of microalgae into value-added products, ChemSusChem (2019), https://doi.org/10.1002/cssc.201901772.
[22] Y. Xin, B. Sun, X. Zhu, Z. Yan, X. Zhao, X. Sun, Hydrogen production from ethanol decomposition by pulsed discharge with needle-net configurations, Appl. Energy 206 (2017) 126–133.
[23] J.T. Franclemont, X. Fan, R. Li, R.K. Singh, T.M. Holsen, S. Mededovic Thagard, Chemical reaction mechanisms accompanying pulsed electrical discharges in liquid methanol, Plasma Process. Polym. 15 (2018) 1800019.
[24] E. Tatarova, N. Bundaleska, F.M. Dias, D. Tsyganov, R. Saavedra, C.M. Ferreira, Hydrogen production from alcohol reforming in a microwave 'tornado'-type plasma, Plasma Sources Sci. Technol. 22 (2013) 065001.
[25] C.C. Chen, H.H. Tseng, W.H. Chen, Hydrogen production and carbon dioxide enrichment from ethanol steam reforming followed by water gas shift reaction, J. Clean. Prod. 162 (2017) 1430–1441.
[26] K.M.K. Yu, W. Tong, A. West, K. Cheung, T. Li, G. Smith, Y. Guo, S.C.E. Tsang, Non-syngas direct steam reforming of methanol to hydrogen and carbon dioxide at low temperature, Nat. Commun. 3 (2012) 1230.
[27] D.C. Upham, V. Agarwal, A. Khechfe, Z.R. Snodgrass, M.J. Gordon, H. Metiu, E.W. McFarland, Catalytic molten metals for the direct conversion of methane to hydrogen and separable carbon, Science 358 (2017) 917–921.
[28] Y. Xin, B. Sun, X. Zhu, Z. Yan, X. Zhao, X. Sun, Carbon nanoparticles production by pulsed discharge in liquid alcohols, Vacuum 151 (2018) 90–95.
[29] P. Vanraes, A. Bogaerts, Plasma physics of liquids-a focused review, Appl. Phys. Rev. 5 (2018) 031103.
[30] Y. Hu, J. Yang, L. Jia, J.S. Yu, Ethanol in aqueous hydrogen peroxide solution: hydrothermal synthesis of highly photoluminescent carbon dots as multifunctional nanosensors, Carbon 93 (2015) 999–1007.
[31] D. Czylkowski, B. Hrycak, M. Jasiński, M. Dors, J. Mizeraczyk, Hydrogen production by direct injection of ethanol microdroplets into nitrogen microwave plasma flame, Int. J. Hydrogen Energy 43 (2018) 21196–21208.
[32] J. Yan, C. Du, Hydrogen Generation from Ethanol Using Plasma Reforming Technology, Springer, 2017.
[33] H. Lange, M. Sioda, A. Huczko, Y. Zhu, H. Kroto, D. Walton, Nanocarbon production by arc discharge in water, Carbon 41 (2003) 1617–1623.
[34] R. Zhou, R. Zhou, S. Wang, Z. Lan, X. Zhang, Y. Yin, S. Tu, S. Yang, L. Ye, Fast liquefaction of bamboo shoot shell with liquid-phase microplasma assisted technology, Bioresour. Technol. 218 (2016) 1275–1278.
[35] X.T. Zhao, X.M. Zhu, Z.Y. Yan, Y.J. Liu, H. Liu, B. Sun, Optical study of active species produced by microwave discharge in water, IEEE Trans. Plasma Sci. 44 (2016) 1369–1374.
[36] L. Wang, W. Li, B. Wu, Z. Li, D. Pan, M. Wu, Room-temperature synthesis of graphene quantum dots via electron-beam irradiation and their application in cell imaging, Chem. Eng. J. 309 (2017) 374–380.
[37] Q. Zhang, S. Deng, J. Liu, X. Zhong, J. He, X. Chen, B. Feng, Y. Chen, K. Ostrikov, Cancer-targeting graphene quantum dots: fluorescence quantum yields, stability, and cell selectivity, Adv. Funct. Mater. 29 (2018) 1805860.
[38] S.Y. Lim, W. Shen, Z. Gao, Carbon quantum dots and their applications, Chem. Soc. Rev. 44 (2015) 362–381.
[39] Y. Hu, J. Yang, J. Tian, J.S. Yu, How do nitrogen-doped carbon dots generate from molecular precursors? An investigation of the formation mechanism and a solution-based large-scale synthesis, J. Mater. Chem. B 3 (2015) 5608–5614.
[40] R. Wang, K.Q. Lu, Z.R. Tang, Y.J. Xu, Recent progress in carbon quantum dots: synthesis, properties and applications in photocatalysis, J. Mater. Chem. A 5 (2017) 3717–3734.
[41] Q. Wang, Q. Zhang, Y. Chen, J. He, K. Jiang, Z. Hu, X. Zhong, Blue luminescent amorphous carbon nanoparticles synthesized by microplasma processing of folic acid, Plasma Process. Polym. 15 (2018) 1700088.